ACS APPLIED NANO MATERIALS

www.acsanm.org Article

# Near-Infrared Electrochemiluminescence of Dual-Stabilizer-Capped Au Nanoclusters for Immunoassays

Hongying Jia, Siqi Yu, Lei Yang, Qin Wei,* and Huangxian Ju*

Cite This: *ACS Appl. Nano Mater.* 2021, 4, 2657−2663 Read Online

ACCESS | Metrics & More | Article Recommendations | Supporting Information



**ABSTRACT:** Surface engineering of electrochemiluminescence (ECL) emitters with capping agents is highly important, yet it remains a challenge. Herein, using *N*-acetyl-L-cysteine and cysteamine as model capping agents, a dual-stabilizer-capped strategy was proposed to achieve red-shifted ECL in the near-infrared region (NIR) via surface engineering water soluble and biocompatible Au nanoclusters (NCs). The dual-stabilizer-capped Au NCs were environment-friendly and exhibited efficient ECL emission at around 860 nm when utilizing triethanolamine as a coreactant, thus providing an NIR ECL tag for bioanalysis in aqueous medium. Benefiting from the low background of NIR emission and the good biocompatibility of the dual-stabilizer-capped Au NCs, a "signal on"-genre NIR ECL immunosensing method was obtained. Then, the immunosensor was established by using the carcinoembryonic antigen as a model analyte and the aforementioned Au NCs as a tag to label the signal antibody, which exhibited a broad linear range from 1 fg/mL to 0.5 ng/mL with a limit of detection of 0.33 fg /mL (S/N = 3). The work offers a method toward deepened understanding of the surface engineering of Au NCs with capping agents for tuning the ECL waveband and developing ECL systems in even longer wavebands.

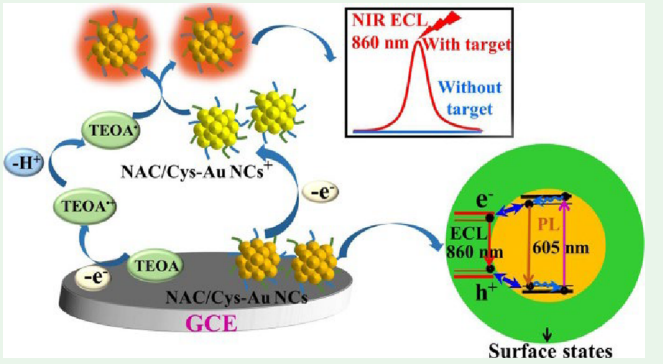


**KEYWORDS:** *near-infrared region, electrochemiluminescence, immunosensors, Au nanoclusters, dual-stabilizer, signal on, carcinoembryonic antigen*

## 1. INTRODUCTION

Electrochemiluminescence (ECL) involves the generation of excited species at appropriate potentials that can relax to the ground state via a light-emitting process.[1,2] It possesses admirable controllability because of the localized response generation at the electrode−solution interface.[3] Since the earliest research on ECL in 1964, screening ECL luminophores has exhibited important impacts on ECL evolution.[4,5] Different luminophores such as luminol,[6] ruthenium complex,[7] $C_3N_4$ nanosheets,[8] and carbon quantum dots[9] have been investigated for ECL emission. Recently, the ECL emission of toxic-element-free polymer dots has attracted tremendous efforts because of their excellent biocompatibility.[10,11] However, the emission of the aforementioned luminophores is confined to the visible range, which limits their application in bioanalysis and bioimaging. Although the emission of semiconductor nanocrystals (CdTe,[12] CdSeTe/ZnS,[13] and PbS),[14] as a group of inorganic ECL emitters, can be extended to the near-infrared (NIR) region, the potential damage of the toxic element-doped nanocrystals also limits its extensive application. Therefore, the metal nanoparticles such as Au nanoclusters (NCs) have nowadays become extensively investigated ECL emitters because of their NIR ECL emission, easy surface modification, good biocompatibility, and environmental friendliness.[15]

Generally, the ECL wavelength of Au NCs can be easily tuned by changing the surface stabilizer. Furthermore, various capping agents of surface modification have been explored for the preparation of luminescent Au NCs, which leads to the ECL emission wavelength of Au NCs from the visible range to the NIR region. For instance, the ECL emission of $H_2N$-MMYYHFRRHL-COOH-capped Au NCs occurs at 475 nm,[16] 6-aza-2-thiothymine capped Au NCs displays a monochromatic ECL process around 532 nm,[17] bovine serum albumin (BSA)-templated Au NCs demonstrate an ECL emission around 650 nm,[18] while methionine-stabilized Au NCs show an NIR ECL emission at 835 nm.[15] The NIR ECL emission possesses unique merits such as large tissue penetration depth, low photochemical hazard, and low background interference, the latter greatly improves the detection sensitivity of target

**Received:** December 8, 2020
**Accepted:** January 21, 2021
**Published:** March 5, 2021

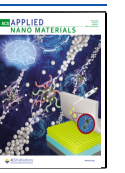

**Scheme 1. Schematic Illustration for the (A) Preparation of $Ab_2$-NAC/Cys-Au NC and (B) Fabrication of the Immunosensor and NIR ECL Immunoassay with NAC/Cys-Au NC as the ECL Tag**

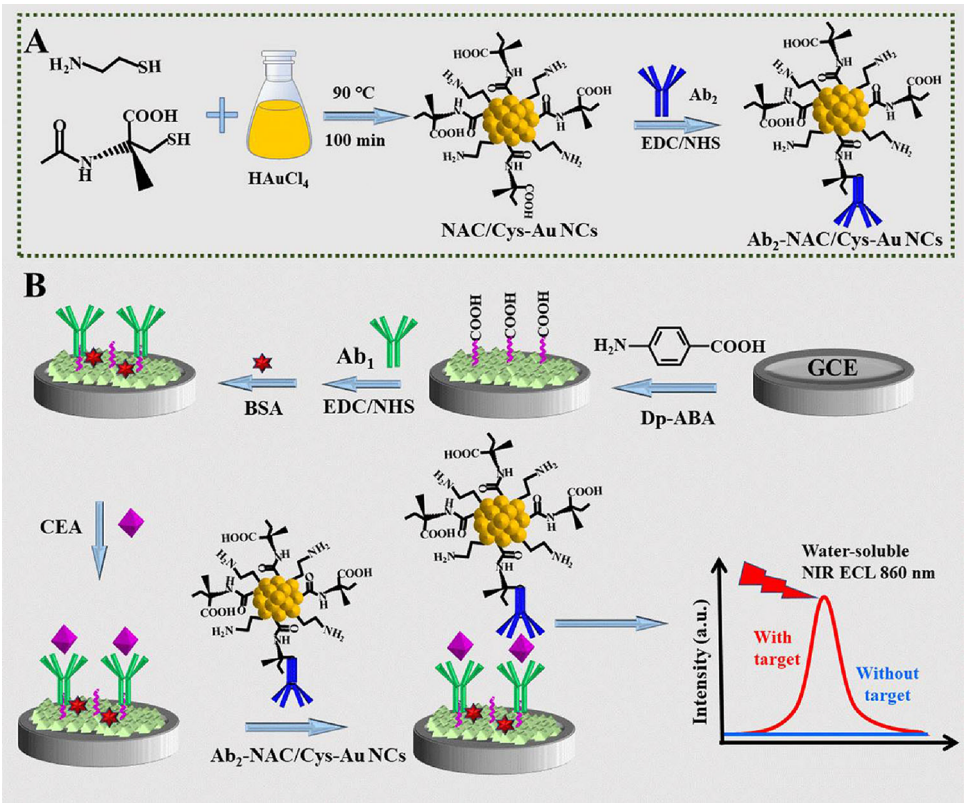


analytes.[19] Meanwhile, the excellent water solubility and stability of Au NCs can be obtained as perfect candidates for ECL emission by applying appropriate stabilizer, which endows the Au NCs with the superiorities of both environmental friendliness and biocompatibility simultaneously. Thus, Au NCs with NIR emission and excellent biocompatibility have attracted continuous attention in biological sensing and imaging.

Herein, we synthesized dual-stabilizer-capped Au NCs with *N*-acetyl-L-cysteine (NAC) and cysteamine (Cys) (NAC/Cys-Au NCs) to realize the excellent performance of NIR ECL emission. The surface state-originated ECL emission of NAC/Cys-Au NCs showed a bathochromic shift of 255 nm in regard to the photoluminescence (PL) emission from the core of NAC/Cys-Au NCs in the aqueous medium.[15] The utilization of dual stabilizers NAC and Cys not only provided Au NCs with outstanding water solubility and biocompatibility, but also achieved the ECL emission at 860 nm in aqueous medium when using triethanolamine (TEOA) as a coreactant. Recently, Au NCs as an NIR ECL luminophor for biomarker detection have shown excellent performances of facile acquisition and hypotoxicity as well as perfect controllability and biocompatibility compared with other luminophors.[20−22] Benefiting from the abovementioned low background of NIR emission and the good biocompatibility, a "signal on"-genre NIR ECL immunosensor was thus developed with NAC/Cys-Au NCs as a labeling tag (Scheme 1). The proposed ECL immunosensor showed a sub-fg/mL-level detection limit for biomarker analysis. The ECL property from NAC/Cys-Au NCs enriches the family of ECL emitters, and provides a promising candidate for ECL bioimaging and wavelength-resolved multiplexing assay with improved performance.

## 2. EXPERIMENTAL SECTION

**2.1. Preparation of NAC/Cys-Au NCs.** All relevant glassware employed in the subsequent processes was rinsed in a fresh solution containing $HNO_3$-HCl (1:3, v/v), and then cleaned thoroughly with ultrapure water and ethanol, and dried for further use. NAC/Cys-Au NCs were synthesized based on the previous researched process with a slight modification (Scheme 1A).[23] In brief, freshly obtained solutions of NAC (30 mM, 0.3 mL) and Cys (30 mM, 0.7 mL) as well as $HAuCl_4$ (10 mg/mL, 1 mL) were injected to 8 mL of ultrapure water. The mixture was incubated at 90 °C for 100 min. Then, the acquired mixture was centrifuged to eliminate the precipitate and then purified with isopropyl alcohol at 13,000 rpm thrice. The obtained NAC/Cys-Au NCs were dissolved in ultrapure water to achieve 1 mg/mL solution and preserved at 4 °C in the dark for further use.

**2.2. Preparation of $Ab_2$-NAC/Cys-Au NCs.** As shown in Scheme 1A, NAC/Cys-Au NC-labeled carcinoembryonic antigen (CEA) $Ab_2$ (i.e., $Ab_2$-NAC/Cys-Au NC) was prepared by mixing 1-ethyl-3-(3-dimethyl-amino-propyl) carbodiimide hydrochloride (EDC) (100 μL, 0.10 mol/L), N-hydroxysuccinimide (NHS) (100 μL, 0.17 mol/L), and NAC/Cys-Au NCs (1 mL, 1 mg/mL) at room temperature (RT) for 30 min to form activated NAC/Cys-Au NCs. The activated NAC/Cys-Au NCs were then centrifuged and commixed with the $Ab_2$ solution (1 mL, 200 μg/mL) under shaking at RT for 8 h. The final compound was centrifuged and re-dispersed in phosphate buffered saline (PBS) (pH 7.4) containing 100 μL of 0.1% BSA for blocking the residual binding sites. After the reaction for 60 min, the dispersion was centrifuged and washed with PBS (pH 7.4) several times, and the as-obtained $Ab_2$-NAC/Cys-Au NC conjugates were dispersed in PBS (1 mL, pH 7.4) and placed at 4 °C for use.

**2.3. Preparation of the Immunosensor and Immunoassay Procedure.** The "signal on"-genre ECL immunosensor was constructed by modifying $Ab_1$ on the glassy carbon electrode (GCE) surface with P-aminobenzoic acid (ABA) for linking.[24,25] The ABA was first immobilized on a pretreated GCE to form GCE-ABA (Scheme 1B).[26] The carboxyl functional groups of ABA on GCE


https://dx.doi.org/10.1021/acsanm.0c03284
ACS Appl. Nano Mater. 2021, 4, 2657−2663

became activated by dropping EDC (20 $\mu$L, 0.52 mol/mL) and NHS (20 $\mu$L, 0.87 mol/mL) for 30 min, which were then incubated with $Ab_1$ (20 $\mu$L, 10 $\mu$g/mL) for 2 h. The GCE-ABA-$Ab_1$ was next washed with PBS and coated with BSA (1%, PBS pH 7.4) for 30 min to block unspecific carboxyl active sites.

The immunoassay was performed through a sandwich-type method. Twenty microliters of CEA solutions with varied concentrations were coated onto the surfaces of the immunosensor and incubated for 2 h at RT. Subsequently, a 10 $\mu$L dispersion of $Ab_2$-NAC/Cys-Au NCs was coated onto the surface and was incubated for 1 h. The resulting sandwich-type immunocomplex modified GCEs were finally used for electrochemical and ECL measurements through the scanning of potential from 0 to +1.6 V at 50 mV/s.

## 3. RESULTS AND DISCUSSION

**3.1. Characterization of NAC/Cys-Au NCs.** The absorption of NAC/Cys-Au NCs exhibited a obvious decline along with increasing wavelength in the ultraviolet range and it had a wide shoulder along with a tail in the visible region (Figure 1A, curve a). No obvious absorption peak was detected

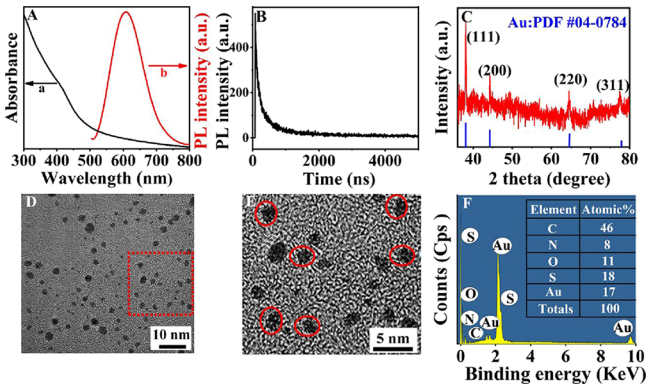


**Figure 1.** (A) UV−vis absorption (a) and PL (b) spectra, (B) PL decay curve,(C) XRD pattern, (D, E) HRTEM images, and (F) EDS pattern of NAC/Cys-Au NCs.

at the wavelengths longer than 520 nm. The absence of the typical surface plasmon resonance peak of Au nanoparticles indicated the subsize of the as-obtained NAC/Cys-Au NCs. The PL spectrum of NAC/Cys-Au NCs exhibited a wide peak together with the maximum emission at 605 nm and the overall width at half-maximum about 150 nm (Figure 1A, curve b). The PL quantum yield of NAC/Cys-Au NCs was about 2.5% and the PL decay curve of NAC/Cys-Au NCs was well matched to a biexponential model along with the PL lifetime of 735.9 ns (Figure 1B and Table S1). The X-ray diffraction (XRD) pattern (Figure 1C) of NAC/Cys-Au NCs exhibited obvious deviations from the PDF#04−0784 Au standard. It demonstrated four characteristic peaks at the 2$\theta$ degree of 38.2, 44.4, 64.6, and 77.5°, which corresponded to (111), (200), (220), and (311) of bulk Au atomic planes, respectively. The NAC/Cys-Au NCs were nearly uniform with the average dimension around 3 nm (Figure 1D,E); meanwhile, it exhibited clear peaks indexed to Au, S, O, N, and C elements on the EDS patterns, respectively (Figure 1F), indicating the formation of Au NCs with the proposed dual-thiols-capped synthetic strategy.

The X-ray photoelectron spectroscopy (XPS) survey spectrum of NAC/Cys-Au NCs (Figure 2A) displayed distinct peaks related to the Au (4f), S (2p), C (1s), N (1s), and O (1s), respectively, which manifested the presence of the

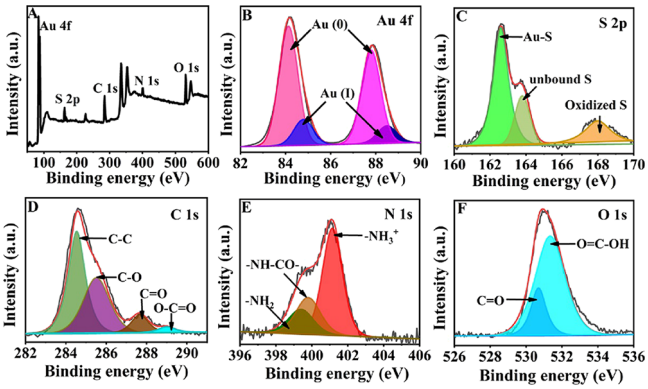


**Figure 2.** (A) XPS survey spectrum of NAC/Cys-Au NCs, and (B-F) XPS spectra of NAC/Cys-Au NCs in Au 4f (B), S 2p (C), C1s(D), N 1 s (E), and O 1 s (F) regions.

stabilizer NAC and Cys on the Au NC surface. Meanwhile, the Au (4f) spectrum (Figure 2B) was deconvoluted into two distinct components centered at 88.0 and 84.4 eV, respectively. The two peaks belonged to Au $4f_{7/2}$ (84.3 eV) and Au $4f_{5/2}$ (87.9 eV) signals of Au (0) and Au $4f_{5/2}$ (88.4 eV) and Au $4f_{7/2}$ (84.7 eV) signals of Au(I), respectively.[27] Additionally, a small amount of Au(I) appeared outside the surface of the Au (0) core, which was also demonstrated to be favorable for the stabilization of the Au NCs, because the remaining Au(I) could form an outer shell to interact strongly with thiolate sulfur atoms.[28−30] As shown in Figure 2C, it was shown that the NAC/Cys-Au NCs were connected with the capping agents via the Au-S covalent binding. The C1s further proved the appearance of NAC and Cys (Figure 2D). Then, as displayed in Figure 2E, two obvious peaks located at 399.5 and 401.2 eV indicated the existence of $-NH_2$ and $-NH_3^+$ groups, and Figure 2F presents different forms of O elements in the dual stabilizer. All these results proved that the NAC and Cys as the capping agents were modified onto the Au NC surface successfully.[23]

**3.2. Electrochemical and ECL Behaviors of NAC/Cys-Au NCs Modified GCE.** The differential pulse voltammetry (DPV) curve of NAC/Cys-Au NCs showed a clear anodic peak at +0.96 V along with the onset potential around +0.47 V in PBS (Figure 3A, right inset), which revealed that NAC/Cys-Au NCs were electrochemically oxidized to positively charged states via hole injection. After scanning from 0 to −1.6 V, an reductive peak was acquired around −1.20 V with the onset potential around −0.85 V (Figure 3A, left inset), indicating that NAC/Cys-Au NCs were electrochemically reduced to negatively charged states through electron injection.

The NAC/Cys-Au NC modified GCE exhibited a weak oxidative peak in PBS, which did not result in a distinct oxidative process and ECL emission (Figure 3, curve a). Upon the addition of TEOA as a coreactant, the oxidative peak greatly increased along with strong ECL emission (Figure 3, curve b), and both the oxidative and emissive peaks occurred at about +1.14 V along with the onset potential at +0.80 V. It was unambiguous that TEOA can be electrochemically oxidized around +0.80 V along with the generation of tremendous reducing TEOA• radicals for electrons injecting into NAC/Cys-Au NCs extensively.[31] The obviously enhanced oxidative process upon introducing TEOA into PBS also indicated that the electrochemical oxidation caused hole


https://dx.doi.org/10.1021/acsanm.0c03284
ACS Appl. Nano Mater. 2021, 4, 2657−2663

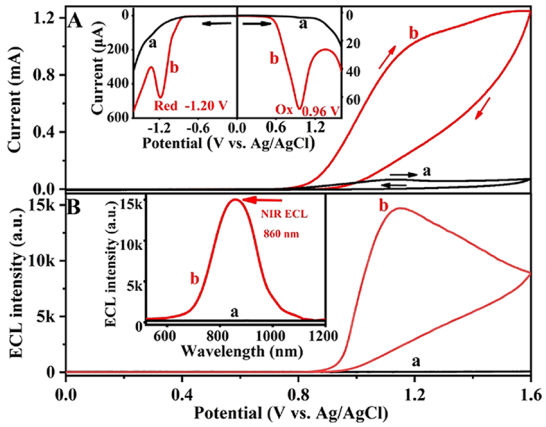


**Figure 3.** (A) CV and (B) ECL-potential profiles of the NAC/Cys-Au NC modified GCE in (a) 0.1 mol/L pH 7.4 PBS and (b) (a) + 0.1 mol/L TEOA. Inset in (A): Cathodic (left) and anodic (right) DPV curves of (a) bare and (b) NAC/Cys-Au NC modified GCEs in $N_2$-saturated 0.1 mol/L PBS (pH 7.4). Inset in (B): ECL spectra of (a) bare and (b) NAC/Cys-Au NC modified GCEs in $N_2$-saturated 0.1 mol/L PBS (pH 7.4) containing 0.1 mol/L TEOA by collecting all the photons generated via scanning the potential from 0 to +1.6 V for one cycle at 50 mV/s.

injection of NAC/Cys-Au NCs, which might be the rate-deciding procedure for the ECL of NAC/Cys-Au NCs.[25]

The ECL spectrum of the NAC/Cys-Au NC modified GCE in the presence of TEOA only exhibited a single peak around 860 nm (Figure 3B, inset), which was 255 nm longer than the PL peak (Figure 1A, curve b), showing an obvious red shift, which might be on account of the different excitation patterns. PL was mainly ascribed to the excitation and emission within the NAC/Cys-Au NC core, while the ECL was attributed to hole−electron recombination process assumed to occur on the NAC/Cys-Au NC surface.[15,32] The large scale of energy bands was attributed to the outside superficial atoms and the wave functions were involved in the states of holes and electrons outside the superficial superpose, which exhibited a narrower band gap than the core.[33,34] The surface engineering of Au NCs with NAC and Cys greatly changed the surface states of Au NCs, which led to the decrease in the difference of band gap on Au NCs, as displayed in Figure S1. As far as we know, this was the longest wavelength of ECL emission observed in an aqueous system. This also demonstrated that the ECL waveband of Au NCs was adjustable by altering their capping agent.[35,36]

A representative reductive−oxidative mechanism could be proposed for the ECL of the NAC/Cys-Au NCs/TEOA system. As displayed in Figure S1, both the hole injection process of NAC/Cys-Au NCs and the electrochemical oxidation process of TEOA had a significant effect on the formation of the reductive-oxidation ECL. Upon anodic potential scanning, the mechanism for ECL of NAC/Cys-Au NCs/GCE with TEOA as the coreactant is proposed in eqs 1−6:

$$\text{NAC/Cys} - \text{Au NCs} \rightarrow n\text{R}^{+\bullet}_{(\text{NAC/Cys}-\text{Au NCs})} + n\text{e}^{-} \quad (1)$$

$$\text{TEOA} \rightarrow \text{TEOA}^{\bullet+} + \text{e}^{-} \quad (2)$$

$$\text{TEOA}^{\bullet+} \rightarrow \text{TEOA}^{\bullet} + \text{H}^{+} \quad (3)$$

$$\text{TEOA}^{\bullet} + \text{NAC/Cys} - \text{Au NCs} \rightarrow \text{R}^{-\bullet}_{(\text{NAC/Cys}-\text{Au NCs})} \quad (4)$$

$$\text{R}^{+\bullet}_{(\text{NAC/Cys}-\text{Au NCs})} + \text{R}^{-\bullet}_{(\text{NAC/Cys}-\text{Au NCs})} \rightarrow \text{R}^{*}_{(\text{NAC/Cys}-\text{Au NCs})} \quad (5)$$

$$\text{R}^{*}_{(\text{NAC/Cys}-\text{Au NCs})} \rightarrow \text{NAC/Cys} - \text{Au NCs} + \text{hv}\ (\sim 860\ \text{nm}) \quad (6)$$

**3.3. Feasibility of ECL Immunosensing.** The surface modification of the GCE for the preparation of the ECL immunosensor was demonstrated through step-by-step cyclic voltammetry (CV) scanning in PBS containing the Fe-$(CN)_6^{3-}$/Fe$(CN)_6^{4-}$ redox couple (Figure S2A).[24,37] The GCE showed a well-shaped CV along with a peak distance of 68 mV (curve a). After the electrochemical deposition of ABA, GCE-ABA showed a dramatic decrease in the peak current and the enlarged peak distance (curve b), which were because of electrostatic repulsion between the negatively charged ferricyanide anion and the negatively charged state of GCE-ABA (ABA pKa = 4.80).[38] After $Ab_1$ was covalently bonded to the surface of GCE-ABA, the peak potential separation decreased along with the appearance of the larger redox peak currents (curve c), indicating the successful covalent modification of $Ab_1$ to GCE-ABA, which decreased the negatively charged surface states of GCE-ABA.[39] However, its incubation with CEA solution for immunoassay decreased the redox peak currents and increased the peak distance again because of the acquisition of immunocomplex GCE-ABA-$Ab_1$ < CEA (curve d), which increased the electron transfer impendence between the electrode and Fe$(CN)_6^{3-}$/Fe-$(CN)_6^{4-}$. The incubation of the GCE-ABA-$Ab_1$ < CEA with the dispersion of $Ab_2$-NAC/Cys-Au NCs further enlarged the peak potential separation and reduced the peak currents (curve e), indicating the formation of a sandwiched immunocomplex GCE-ABA-$Ab_1$ < CEA>$Ab_2$-NAC/Cys-Au NCs, which blocked the electron transfer process.

Meanwhile, the ECL signals also demonstrated the surface immunoreactions (Figure S2B). The bare GCE, GCE-ABA, GCE-ABA-$Ab_1$, and GCE-ABA-$Ab_1$ < CEA did not show any ECL emission in PBS containing TEOA (curves a-d), and the formation of GCE-ABA-$Ab_1$ < CEA>$Ab_2$-NAC/Cys-Au NCs led to an obvious ECL signal with a peak potential of +1.10 V (curve e), which not only indicated that NAC/Cys-Au NCs were successfully immobilized onto the GCE surface through the processes described above, but also manifested that $Ab_2$ preserved its bioactivity on NAC/Cys-Au NCs, providing a novel immunosensing means for ECL detection of the target.

**3.4. Optimization of Detection Conditions.** The pH value was significant for the ECL intensity of the obtained immunosensor (Figure 4A). After exploring the performance of the immunosensor along with the increased pH values from 5.4 to 8.6, the neutral value (pH 7.4) was acquired as the optimal pH. TEOA was used as the coreactant of NAC/Cys-Au NCs, and the ECL intensity obtained the optimal performance, when the concentration of TEOA was 0.1 mol/L (Figure 4B). Furthermore, the incubation time of $Ab_2$ bioconjugates is displayed in Figure 4C, and the performance showed an optimal incubation time of 480 min. The performance for the immunosensor with amino-group containing coreactants (TEOA, TEA, TPrA, DBAE, and $N_2H_4.H_2O$) and amino-group excluding coreactants ($K_2C_2O_4$


https://dx.doi.org/10.1021/acsanm.0c03284
ACS Appl. Nano Mater. 2021, 4, 2657−2663

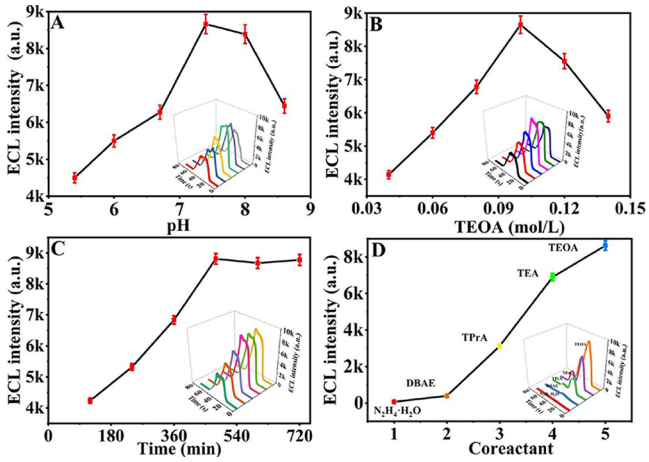


**Figure 4.** (A) Effects of pH, (B) TEOA coreactant concentration, (C) incubation time of $Ab_2$, and (D) different coreactants at 0.10 mol/L on ECL intensity. Error bars = SD ($n$ = 3)

and $H_2O_2$) is shown in Figure 4D and Figure S3; it is undisputed that TEOA is the most efficient coreactant.

**3.5. Performance of the ECL Immunosensing Method for CEA.** Under the optimal condition, the strong ECL signal of GCE-ABA-$Ab_1$ < CEA>$Ab_2$-NAC/Cys-Au NCs in PBS possessing TEOA increased with the enhanced CEA concentration (Figure 5A). The plot of ECL response versus the logarithmic value of CEA concentration showed an excellent linear relationship in the concentration range from 1 fg/mL to 0.5 ng/mL ($R^2$ = 0.996) (Figure 5B). The limit of detection (LOD) was calculated to be 0.33 fg/mL at an S/N of 3, which should be the lowest LOD for CEA immunoassay

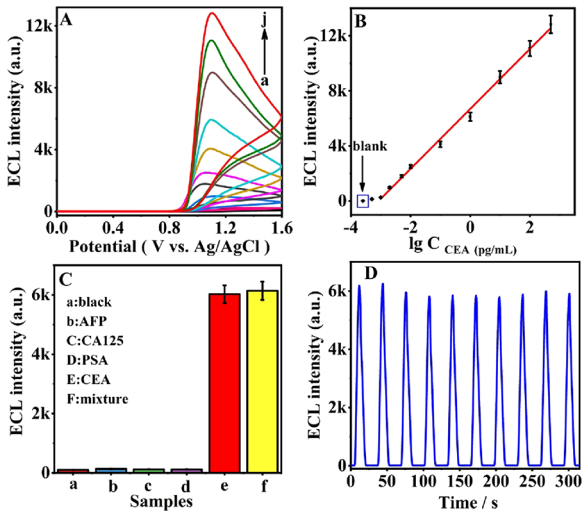


**Figure 5.** (A) ECL responses of the immunosensor to 0, 1.0, 2.0, 5.0, 10, 100 fg/mL, 1.0, 10, 100, and 500 pg/mL CEA (from a to j), (B) the corresponding calibration curve for CEA determination by scanning the potential from 0 to +1.6 V in 0.1 mol/L PBS containing 0.1 mol/L TEOA at 50 mV/s, (C) selectivity of the proposed CEA biosensor toward (a) blank, (b) 100 pg/mL AFP, (c) 100 pg/mL CA125, (d) 100 pg/mL PSA, (e) 1.0 pg/mL CEA, and (f) the mixture containing 1.0 pg/mL CEA, 100 pg/mL AFP, 100 pg/mL CA125, and 100 pg/mL PSA, and(D) reproducibility of the proposed CEA biosensor upon continuously cycling from 0 to +1.6 V in 0.1 mol/L PBS containing 0.1 mol/L TEOA .

(Table S2) because of the NIR ECL emission of NAC/Cys-Au NCs.

**3.6. Specificity, Reproducibility, and Stability of ECL Immunosensing.** The selectivity, reproducibility, and stability are significant parameters to evaluate the performance of the fabricated immunosensors. The specificity of the proposed immunosensing method was examined with conventional disturbing proteins, such as AFP, CA125, and PSA, at the content 100 times that of CEA (Figure 5C). Compared to the strong ECL signal in the presence of 1.0 pg/mL CEA (column e), all ECL signals for interfering samples containing 100 pg/mL proteins were negligible, similar to that of the blank solution (columns a-e). Significantly, the mixture 1.0 pg/mL CEA with 100 pg/mL AFP, 100 pg/mL CA125, and 100 pg/mL PSA (column f) exhibited an insignificant difference from that of 1 pg/mL CEA alone (column e). It was distinct that the coexisting AFP, CA125, and PSA did not interfere with the determination of CEA, and the fabricated ECL immunosensor for CEA exhibited approving selectivity. The immunosensor proved an acquirable ECL intensity along with cycling scanning between 0 to +1.6 V in PBS including 0.1 mol/L TEOA (Figure 5D). The relative standard deviation (RSD) of the ECL intensity was 2.6% for 10 cycles, which illustrated good reproducibility of the ECL immunosensor. The stability was measured by shelving the constructed immunosensor for 7 days, and the intensity was 95% of the original intensity, which indicated acceptable performance.

**3.7. Real Sample Analysis.** With the aim of verifying the actual application of the fabricated immunosensor, real sample analysis is necessary. Human serum was acquired from the school hospital and diluted thrice. The CEA concentration was tested to be 10 pg/mL with the obtained immunosensor. Then different concentrations of CEA (10, 40, and 90 pg/mL) were injected to the aforementioned serum for the test. As shown in Table 1, the recovery was from 97.6 to 102.2 and the RSD was from 1.8 to 4.2% ($n$ = 5).

**Table 1. Recovery Results Acquired from Serum of CEA Applying the Proposed ECL Immunosensor**

| initial content (pg/mL) | added content (pg/mL) | found content(pg/mL) | RSD($n$ = 5, %) | recovery(%) |
|---|---|---|---|---|
| | 10 | 19.1, 20.7, 20.6, 20.3, 21.5 | 4.2 | 102.2 |
| 10 | 40 | 48.7, 49.5, 48.3, 47.9, 50.1 | 1.8 | 97.6 |
| | 90 | 98.2, 100.9, 104.7, 97.2, 103.8 | 3.3 | 101 |

## 4. CONCLUSIONS

A dual-stabilizer-capped strategy for red-shifted ECL emission and the synthesis of the NIR ECL luminophore was designed in this work. The NAC/Cys-Au NCs exhibit efficient ECL emission at around 860 nm when utilizing TEOA as a coreactant, which is 255 nm longer than the PL emission from the Au NC core and the longest wavelength of ECL emission from the surface states of Au NCs in aqueous medium. Because of the low background of NIR emission and the good biocompatibility, an ultrasensitive NIR ECL immunoassay has been proposed by using the Au NCs as a tag to label the signal antibody. The excellent performance of the proposed method demonstrates that the strategy for surface engineering of Au


https://dx.doi.org/10.1021/acsanm.0c03284
ACS Appl. Nano Mater. 2021, 4, 2657−2663

NCs to acquire NIR ECL shows great promise in developing ECL systems and enhancing the throughput of the wavelength-resolved multiplexing ECL analysis and bioimaging.

## ■ ASSOCIATED CONTENT

### Supporting Information

The Supporting Information is available free of charge at https://pubs.acs.org/doi/10.1021/acsanm.0c03284.

Chemicals and materials; apparatus; PL Life time parameters of NAC/Cys-Au NCs; schematic illustration of PL and ECL emission mechanisms; feasibility of ECL immunosensing; ECL-potential performance of the immunosensor with amino-group free coreactants ($K_2C_2O_4$ and $H_2O_2$); analytical performances of comparable methods for CEA detection (PDF).

## ■ AUTHOR INFORMATION


### Corresponding Authors

**Qin Wei** − *Collaborative Innovation Center for Green Chemical Manufacturing and Accurate Detection, Key Laboratory of Interfacial Reaction & Sensing Analysis in Universities of Shandong, School of Chemistry and Chemical Engineering, University of Jinan, Jinan 250022, P. R. China;* orcid.org/0000-0002-3034-8046; Phone: +86-25-89683593; Email: sdjndxwq@163.com

**Huangxian Ju** − *Collaborative Innovation Center for Green Chemical Manufacturing and Accurate Detection, Key Laboratory of Interfacial Reaction & Sensing Analysis in Universities of Shandong, School of Chemistry and Chemical Engineering, University of Jinan, Jinan 250022, P. R. China; State Key Laboratory of Analytical Chemistry for Life Science, College of Chemistry and Chemical Engineering, Nanjing University, Nanjing 210023, P. R. China;* orcid.org/0000-0002-6741-5302; Email: hxju@nju.edu.cn

### Authors

**Hongying Jia** − *Collaborative Innovation Center for Green Chemical Manufacturing and Accurate Detection, Key Laboratory of Interfacial Reaction & Sensing Analysis in Universities of Shandong, School of Chemistry and Chemical Engineering, University of Jinan, Jinan 250022, P. R. China*

**Siqi Yu** − *State Key Laboratory of Analytical Chemistry for Life Science, College of Chemistry and Chemical Engineering, Nanjing University, Nanjing 210023, P. R. China*

**Lei Yang** − *Collaborative Innovation Center for Green Chemical Manufacturing and Accurate Detection, Key Laboratory of Interfacial Reaction & Sensing Analysis in Universities of Shandong, School of Chemistry and Chemical Engineering, University of Jinan, Jinan 250022, P. R. China*

Complete contact information is available at: https://pubs.acs.org/10.1021/acsanm.0c03284


### Author Contributions

H.J. conceptualized the proposal and wrote the original-draft. S.Y. helped review the draft. L.Y. helped review the data. Q.W. offered funding support and supervision. H.J. offered funding support and supervision.

### Notes

The authors declare no competing financial interest.

## ■ ACKNOWLEDGMENTS

This project was supported by the National Natural Science Foundation of China (21627809 and 21827812), the Special Foundation for Taishan Scholar Professorship of Shandong Province (No. TS201712052), and the Innovation Team Project of Colleges and Universities in Jinan (No. 2019GXRC027).

## ■ REFERENCES


(1) Chen, S.; Ma, H. D.; Padelford, J. W.; Qinchen, W. L.; Yu, W.; Wang, S. X.; Zhu, M. Z.; Wang, G. L. Near Infrared Electrochemiluminescence of Rod-Shape 25-Atom AuAg Nanoclusters That Is Hundreds-Fold Stronger Than That of $Ru(bpy)_3$ Standard. *J. Am. Chem. Soc.* **2019**, *141*, 9603−9609.

(2) Richter, M. Electrochemiluminescence (ECL). *Chem. Rev.* **2004**, *106*, 3003−3036.

(3) Tan, J.; Xu, L. R.; Li, T.; Su, B.; Wu, J. M. Image-Contrast Technology Based on the Electrochemiluminescence of Porous Silicon and Its Application in Fingerprint Visualization. *Angew. Chem., Int. Ed.* **2014**, *53*, 9822−9826.

(4) Hercules, D. M. Chemiluminescence Resulting from Electrochemically Generated Species. *Science* **1964**, *145*, 808−809.

(5) Robert, E.; Visco, A. E. A. C. Electroluminescence in Solutions of Aromatic Hydrocarbons. *J. Am. Chem. Soc.* **1964**, *86*, 5350.

(6) Yang, L.; Jia, Y.; Wu, D.; Zhang, Y.; Ju, H. X.; Du, Y.; Ma, H. M.; Wei, Q. Synthesis and Application of $CeO_2/SnS_2$ Heterostructures as a Highly Efficient Coreaction Accelerator in the Luminol-Dissolved $O_2$ System for Ultrasensitive Biomarkers Immunoassay. *Anal. Chem.* **2019**, *91*, 14066−14073.

(7) Zhao, G. H.; Wang, Y. G.; Li, X. J.; Yue, Q.; Dong, X.; Du, B.; Cao, W.; Wei, Q. Dual-Quenching Electrochemiluminescence Strategy Based on Three-Dimensional Metal-Organic Frameworks for Ultrasensitive Detection of Amyloid-beta. *Anal. Chem.* **2019**, *91*, 1989−1996.

(8) Cheng, C. M.; Huang, Y.; Wang, J.; Zheng, B. Z.; Yuan, H. Y.; Xiao, D. Anodic Electrogenerated Chemiluminescence Behavior of Graphite-like Carbon Nitride and Its Sensing for Rutin. *Anal. Chem.* **2013**, *85*, 2601−2605.

(9) Zheng, L. Y.; Chi, Y. W.; Dong, Y. Q.; Lin, J. P.; Wang, B. B. Electrochemiluminescence of Water-Soluble Carbon Nanocrystals Released Electrochemically from Graphite. *J. Am. Chem. Soc.* **2009**, *131*, 4564−4565.

(10) Wang, N. N.; Feng, Y. Q.; Wang, Y. W.; Ju, H. X.; Yan, F. Electrochemiluminescent Imaging for Multi-Immunoassay Sensitized by Dual DNA Amplification of Polymer Dot Signal. *Anal. Chem.* **2018**, *90*, 7708−7714.

(11) Wang, N. N.; Wang, Z. Y.; Chen, L. Z.; Chen, W. W.; Quan, Y. W.; Cheng, Y. X.; Ju, H. X. Dual Resonance Energy Transfer in Triple-component Polymer Dots to Enhance Electrochemiluminescence for Highly Sensitive Bioanalysis. *Chem. Sci.* **2019**, *10*, 6815−6820.

(12) He, Y. P.; Zhang, F.; Zhang, B.; Zou, G. Z. Dichroic Mirror-Assisted Electrochemiluminescent Assay for Simultaneously Detecting Wild-type and Mutant p53 with Photomultiplier Tubes. *Anal. Chem.* **2018**, *90*, 5474−5480.

(13) Stewart, A. J.; Brown, K.; Dennany, L. Cathodic Quantum Dot Facilitated Electrochemiluminescent Detection in Blood. *Anal. Chem.* **2018**, *90*, 12944−12950.

(14) Hesari, M.; Swanick, K. N.; Lu, J. S.; Whyte, R.; Wang, S. N.; Ding, Z. F. Highly Efficient Dual-Color Electrochemiluminescence from BODIPY-Capped PbS Nanocrystals. *J. Am. Chem. Soc.* **2015**, *137*, 11266−11269.

(15) Yu, L.; Zhang, Q.; Kang, Q.; Zhang, B.; Shen, D. Z.; Zou, G. Z. Near-Infrared Electrochemiluminescence Immunoassay with Biocompatible Au Nanoclusters as Tags. *Anal. Chem.* **2020**, *92*, 7581−7587.

(16) Jia, Y.; Liu, S. H.; Du, Y.; Yang, L.; Liu, X. J.; Liu, L.; Ren, X.; Wei, Q.; Ju, H. X. Intramolecular Coreaction Accelerated Electrochemiluminescence of Polypeptide-Biomineralized Gold Nanoclusters

for Targeted Detection of Biomarkers. *Anal. Chem.* **2020**, *92*, 9179−9187.
(17) Yang, L. Q.; Zhang, B.; Fu, L.; Fu, K. N.; Zou, G. Z. Efficient and Monochromatic Electrochemiluminescence of Aqueous-Soluble Au Nanoclusters via Host-Guest Recognition. *Angew. Chem., Int. Ed.* **2019**, *58*, 6901−6905.
(18) Zhou, Y.; Chen, S. H.; Luo, X. L.; Chai, Y. Q.; Yuan, R. Ternary Electrochemiluminescence Nanostructure of Au Nanoclusters as a Highly Efficient Signal Label for Ultrasensitive Detection of Cancer Biomarkers. *Anal. Chem.* **2018**, *90*, 10024−10030.
(19) Liu, J. L.; Zhang, J. Q.; Tang, Z. L.; Zhuo, Y.; Chai, Y. Q.; Yuan, R. Near-infrared Aggregation-Induced Enhanced Electrochemiluminescence from Tetraphenylethylene Nanocrystals: a New Generation of ECL Emitters. *Chem. Sci.* **2019**, *10*, 4497−4501.
(20) Wang, X.; Shang, L.; Zhang, W.; Jia, L. P.; Ma, R. N.; Jia, W. L.; Wang, H. S. An Ultrasensitive Luminol Cathodic Electrochemiluminescence Probe with Highly Porous Pt on Ionic Liquid Functionalized Graphene Film as Platform for Carcinoembryonic Antigen Sensing. *Biosens. Bioelectron.* **2019**, *141*, No. 111436.
(21) Wang, X. M.; Zhang, Q.; Kang, Q.; Zou, G. Z.; Shen, D. Z. A High Sensitive Single Luminophore Ratiometric Electrochemiluminescence Immunosensor in Combined with Anodic Stripping Voltammetry. *Electrochim. Acta* **2020**, *336*, No. 135725.
(22) Zhang, W.; Song, Y.; He, S. J.; Shang, L.; Ma, R. N.; Jia, L. P.; Wang, H. S. Perylene Diimide as a Cathodic Electrochemiluminescence Luminophore for Immunoassays at Low Potentials. *Nanoscale* **2019**, *11*, 20910−20916.
(23) Deng, H. H.; Huan, K. Y.; He, S. B.; Xue, L. P.; Peng, H. P.; Zha, D. J.; Sun, W. M.; Xia, X. H.; Chen, W. Rational Design of High-Performance Donor-Linker-Acceptor Hybrids Using a Schiff Base for Enabling Photoinduced Electron Transfer. *Anal. Chem.* **2020**, *92*, 2019−2026.
(24) Zhang, B.; Zhang, F.; Zhang, P.; Shen, D. Z.; Gao, X. W.; Zou, G. Z. Ultrasensitive Electrochemiluminescent Sensor for MicroRNA with Multinary Zn-Ag-In-S/ZnS Nanocrystals as Tags. *Anal. Chem.* **2019**, *91*, 3754−3758.
(25) Long, X. Y.; Zhang, F.; He, Y. P.; Hou, S. F.; Zhang, B.; Zou, G. Z. Promising Anodic Electrochemiluminescence of Nontoxic Core/Shell $CuInS_2$/ZnS Nanocrystals in Aqueous Medium and Its Biosensing Potential. *Anal. Chem.* **2018**, *90*, 3563−3569.
(26) Zhang, X.; Tan, X.; Zhang, B.; Miao, W. J.; Zou, G. Z. Spectrum-Based Electrochemiluminescent Immunoassay with Ternary CdZnSe Nanocrystals as Labels. *Anal. Chem.* **2016**, *88*, 6947−6953.
(27) Jiang, X. F.; Wang, X. Y.; Yao, C.; Zhu, S. X.; Liu, L.; Liu, R. H.; Li, L. D. Surface-Engineered Gold Nanoclusters with Biological Assembly-Amplified Emission for Multimode Imaging. *J. Phys. Chem. Lett.* **2019**, *10*, 5237−5243.
(28) Xie, J. P.; Zheng, Y. G.; Ying, J. Y. Protein-Directed Synthesis of Highly Fluorescent Gold Nanoclusters. *J. Am. Chem. Soc.* **2009**, *131*, 888−889.
(29) Negishi, Y. N. Katsuyuki. Tsukuda, Tatsuya. Glutathione-Protected Gold Clusters Revisited: Bridging the Gap between Gold(I)-Thiolate Complexes and Thiolate-Protected Gold Nanocrystals. *J. Am. Chem. Soc.* **2005**, *127*, 5261−5270.
(30) Whetten, R. L.; Price, R. C. Nano-Golden Order. *Science* **2007**, *318*, 407−408.
(31) Qin, X. L.; Gu, C. Y.; Wang, M. H.; Dong, Y. F.; Nie, X.; Li, M. X.; Zhu, Z. W.; Yang, D.; Shao, Y. H. Triethanolamine-Modified Gold Nanoparticles Synthesized by a One-Pot Method and Their Application in Electrochemiluminescent Immunoassay. *Anal. Chem.* **2018**, *90*, 2826−2832.
(32) Valenti, G.; Rampazzo, E.; Kesarkar, S.; Genovese, D.; Fiorani, A.; Zanut, A.; Palomba, F.; Marcaccio, M.; Paolucci, F.; Prodi, L. Electrogenerated Chemiluminescence from Metal Complexes-Based Nanoparticles for Highly Sensitive Sensors Applications. *Coord. Chem. Rev.* **2018**, *367*, 65−81.
(33) Wu, P.; Hou, X. D.; Xu, J. J.; Chen, H. Y. Electrochemically Generated Versus Photoexcited Luminescence from Semiconductor Nanomaterials: Bridging the Valley Between Two Worlds. *Chem. Rev.* **2014**, *114*, 11027−11059.
(34) Ding, Z. F.; Quinn, B. M.; Haram, S. K.; Pell, L. E.; Korgel, B. A.; Bard, A. J. Electrochemistry and Electrogenerated Chemiluminescence from Silicon Nanocrystal Quantum dots. *Science* **2002**, *296*, 1293−1297.
(35) Kim, J. M.; Jeong, S.; Song, J. K.; Kim, J. Near-infrared Electrochemiluminescence from Orange Fluorescent Au Nanoclusters in Water. *Chem. Commun.* **2018**, *54*, 2838−2841.
(36) Peng, H. P.; Jian, M. L.; Deng, H. H.; Wang, W. J.; Huang, Z. N.; Huang, K. Y.; Liu, A. L.; Chen, W. Valence States Effect on Electrogenerated Chemiluminescence of Gold Nanocluster. *ACS Appl. Mater. Interfaces* **2017**, *9*, 14929−14934.
(37) Li, Z. Y.; Lin, Z. F.; Wu, X. Y.; Chen, H. T.; Chai, Y. Q.; Yuan, R. Highly Efficient Electrochemiluminescence Resonance Energy Transfer System in One Nanostructure: Its Application for Ultrasensitive Detection of MicroRNA in Cancer Cells. *Anal. Chem.* **2017**, *89*, 6029−6035.
(38) Liu, S. F.; Zhang, X.; Yu, Y. M.; Zou, G. Z. A Monochromatic Electrochemiluminescence Sensing Strategy for Dopamine with Dual-Stabilizers-Capped CdSe Quantum Dots as Emitters. *Anal. Chem.* **2014**, *86*, 2784−2788.
(39) Zhang, X.; Zhang, B.; Miao, W. J.; Zou, G. Z. Molecular-Counting-Free and Electrochemiluminescent Single-Molecule Immunoassay with Dual-Stabilizers-Capped CdSe Nanocrystals as Labels. *Anal. Chem.* **2016**, *88*, 5482−5488.


https://dx.doi.org/10.1021/acsanm.0c03284
*ACS Appl. Nano Mater.* 2021, 4, 2657−2663